ACS APPLIED NANO MATERIALS

www.acsanm.org Article

Soot-Derived Flash Graphene as Cement Additive

Wala A. Algozeeb, Ali Algadhib, Shamsad Ahmad,* Mohammed A. Al-Osta, Ashraf A. Bahraq, Weiyin Chen, Syed Khaja Najamuddin, Syed Imran Ali, and James M. Tour*

Cite This: https://doi.org/10.1021/acsanm.4c05322 Read Online

ACCESS | Metrics & More | Article Recommendations | Supporting Information

ABSTRACT: The incorporation of graphene-based materials into cement composites is one of many interesting nano-reinforcement techniques. However, the conventional production of graphene materials usually requires large quantities of solvent with energy-intensive mixing, which in turn restricts their commercial viability in cement and concrete applications. In this study, an approach for production of flash graphene (FG) from motor oil soot and diesel particulate using a Joule heating system was developed. A high-quality FG was obtained, as evident from Raman spectroscopy analysis. The FG product was added to a mixture to reinforce its microstructure. The results of the mechanical tests conducted on the cement mortar reinforced by admixing 0.1 wt % FG showed an increase in compressive, tensile, and flexural strengths and modulus of elasticity by 38%, 27%, 27%, and 34%, respectively, after curing for 28 days. The durability characteristics in terms of water absorption showed a slightly higher resistance of the FG-reinforced mortar to water penetration. The drying shrinkage of the FG-reinforced mortar was like that of the control mixture. A molecular dynamics simulation was performed on the cured FG-reinforced cement mortar to find that the Ca−Si interactions in the hydrated cement phase were boosted by the presence of FG, in addition to the strong interaction between the Ca and FG sheets. This study could contribute toward developing strong and sustainable nano-reinforced cementitious composites using graphene materials derived from inexpensive carbon and waste sources.

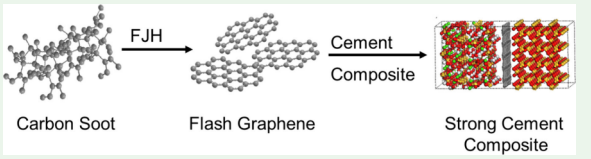

KEYWORDS: *flash graphene, cementitious composites, mechanical properties, durability, nanoengineering, molecular dynamics*

INTRODUCTION

The use of nanomaterials in cement and concrete materials has been widely accepted as an emerging approach to the enhancement of concrete properties. Among these materials, graphene and its derivatives, such as graphene oxide (GO), reduced graphene oxide (rGO), and pristine graphene (PRG), have been reported to possess unique characteristics.[1,2] In particular, graphene has high tensile strength, Young's modulus, tension rigidity, and flexural rigidity of 130 GPa, 1 TPa, 340 GPa·nm, and 3.18 GPa·nm^3, respectively, making it a candidate additive for cement.[3−5] Moreover, graphene-derived composites have been reported to have superior properties.[6−8]

Several studies have been reported on reinforcing cement and concrete mixtures with graphene sheets.[6,7,9] Enhancement in the compressive and tensile strength has been observed upon GO inclusion.[7,9] The transport characteristics of GO-reinforced cement composites were investigated to reveal that GO addition to concrete refines the microstructure of the composite, thereby enhancing the water sorptivity and chloride penetration.[10] Similarly, surfactant-functionalized graphene−concrete mixtures were found to improve compressive, tensile, and flexural strengths.[1] However, the durability characteristics in terms of water absorption and shrinkage revealed a negative impact of graphene on the durability performance of concrete. Furthermore, the addition of GO to fly ash-slag-based geopolymer concrete has been investigated to show enhancement in its properties.[11,12] Therefore, the incorporation of graphene nanomaterials into the cement and concrete mixtures is a promising route to improve the hydration process as well as the mechanical properties.[13−17]

Despite improvements in concrete−graphene composites' properties and performance, one of the barriers to commercializing their use in large-scale applications and infrastructures is the production cost of graphene-based materials. Prior graphene production routes required the use of costly strong acids or organic solvents, which resulted in a high overall cost for graphene.[9,18−20] Recently, an approach to produce high-quality graphene using a flash Joule heating (FJH) system of inexpensive carbon sources, such as coal,[21] petroleum coke,[21,22] carbon black,[21] plastic waste,[23] and rubber tires,[24] was reported. The process is catalyst-free, solvent-free, and scalable and requires no furnaces, solvents, or reactive gases.[21] FJH requires only electricity, which can be supplied from green and renewable sources. Thus, this emerging graphene production technology provides an inexpensive graphene product for possible large-scale applications such as building

Received: September 16, 2024
Revised: October 16, 2024
Accepted: October 17, 2024

https://doi.org/10.1021/acsanm.4c05322
ACS Appl. Nano Mater. XXXX, XXX, XXX−XXX

material composites. FG has been tested as a cement additive, showing superior enhancement in properties of FG−cement composites compared to conventionally exfoliated graphene materials, since small fractions of FG can significantly improve the mechanical strength of the cement composites.[21] Additional studies on FG inclusion in cement mortar systems where sand is incorporated are important.

The application of MD simulations to cement−graphene composites provides a molecular-level understanding of the interactions and behaviors of these materials. This information is invaluable for guiding experimental efforts, optimizing composite designs, and tailoring properties for specific applications in construction and other fields. However, most of the reported MD studies focused only on the graphene-hydrated cement interaction and ignored the presence of the sand phase. Therefore, the present study attempts to simulate the whole mortar mixture encompassing calcium silicate hydrate, silica from the sand, and flash graphene from motor oil soot (MOS).

With the continuation of the efforts to reduce the environmental impact of large-scale industries, the enhancement of materials' performance is a key aspect of minimizing the industrial carbon footprint. In this work, negative value carbon wastes from MOS and diesel particles (DP) were converted to flash graphene (FG), which can be used for large-scale applications. To our knowledge, the use of FG derived from motor oil soot (MOS-FG) in a cement mortar has not yet been explored. Thus, the resultant MOS-FG was used as an additive to a cement mortar mixture to demonstrate the possibility of converting soot from combustion processes to useful FG. Mechanical properties such as compressive strength, splitting tensile strength, flexural strength, and modulus of elasticity were tested. Water absorption and shrinkage tests were also conducted. In addition, a molecular dynamics simulation was performed to understand the fundamental mechanism of graphene reinforcement in cement composites. The laboratory investigation and molecular dynamics provide a comprehensive evaluation of the FG−cement composite.

EXPERIMENTAL METHODS

Preparation of the Carbon Materials. MOS was prepared by combusting motor oil and collecting the soot in a jar placed on top of the burning oil. The yield of soot was found to be ∼1%. Diesel particulates were collected from diesel particulate filters from a local truck yard in Houston, TX, USA.

Flash Graphene Synthesis. A 0.15−0.25 g portion of the soot powder was packed between two copper electrodes in quartz tubes (tube thickness: 2 mm, inner diameter: 8 mm, length: 5 cm). The samples were compressed to obtain a resistivity of ≤500 Ω for ∼0.25 g of soot. Samples were pretreated by subjecting the carbon to low-voltage flashes 5× at 100 V. A capacitor bank consisting of 10 capacitors with a nominal voltage and a total capacitance of 450 V and 60 mF, respectively, was charged to 110 V. The system is designed to allow a discharge time of 500 ms, which is the time the circuit remained open; the flash is much faster. The discharge time allows us to achieve high-quality graphene (see SI for safety guidelines). The FJH reactor is described in our previous work.[21,24] The temperature was measured using an infrared (IR) thermometer (Micro-Epsilon) with a time resolution of 1 ms.

Flash Graphene Characterization. A series of microstructural analyses were carried out to characterize the produced FG. Raman spectroscopy was carried out using a Renishaw Raman microscope and a 532 nm laser with a power of 5 mW. X-ray diffraction (XRD) was performed using a Rigaku D/Max Ultima II powder XRD. The sample for transmission electron microscopy (TEM) analysis was prepared by dropping diluted dispersions (∼1 mg mL^{-1} in isopropanol) of the graphene (<200 μL) on the TEM Cu grids. The TEM was carried out using a JEOL 2100F field-emission gun TEM at 200 kV. A PHI Quantera SXM scanning X-ray microprobe having a base pressure of 5×10^{-9} Torr was used to collect XPS data. The survey and elemental spectra were recorded using 0.5 eV and 0.1 eV steps with a pass energy of 140 eV and 26 eV, respectively.

Mortar Preparation. Ordinary Portland cement (OPC) conforming to ASTM C150[25] with a specific gravity of 3.15 was used. The chemical composition of the OPC is shown in Table 1. Dune sand, having a fineness modulus of 1.85 and a specific gravity of 2.62 in saturated surface dry conditions, was used as a fine aggregate (FA). Two mortar mixes were prepared with sand/cement and water/cement ratios of 2.75 and 0.45, respectively. The first mixture was prepared using 100% OPC as a precursor material, while the second one was admixed with 0.1% FG by weight of cement. The detailed mixture proportions are summarized in Table 2.

Table 1. Chemical Compositions of OPC

Chemical composition	Weight (%)
SiO_2	20.7
Al_2O_3	5.7
Fe_2O_3	2.3
CaO	64.8
MgO	1.1
SO_3	3.21

Table 2. Mix Proportions of Mortars.

Mix ID	OPC (kg/m^3)	FG (kg/m^3)	Water (kg/m^3)	Sand (kg/m^3)	Flow Values (%)
M1-ref	543	0	244.34	1493.2	56.9 ± 1.3
M2-FG	543	0.54	244.34	1493.2	49.6 ± 0.8

Initially, the FG was dispersed in the total water required for the mix using a sonicator. Sonication was performed at 60% amplitude (50 W) for 30 min. A Hobart planetary mixer was used to mix the materials. The FG dispersions were mixed with cement in a mixer for 3 min. Sand was then introduced into the mixer, and mixing was continued for 5 min, making sure that the mix was homogeneous. The mortar mixtures were cast in the molds. The composites were demolded after 24 h and kept in a water curing tank for 7 and 28 days at a temperature of 23 ± 1 °C.

Testing of Mortar Composites. Before being cast into molds, the mortar flow was measured using a flow table test in accordance with ASTM C1437.[26] The compressive strength of mortar composites was determined on 50 mm × 50 mm × 50 mm cubes using a digital compression testing machine, MATEST C55, as per ASTM C109.[27] The compression load was applied at a rate of 1.0 kN/s until failure. The flexural capacity of mortar specimens was also tested using the four-point bending test as per ASTM C78.[28] The test was conducted by using an Instron universal testing machine of 600 kN capacity, and the load was applied constantly without shock at a rate of 0.5 N/min until the composite ruptured. Splitting tensile strength was determined according to ASTM C496[29] using a digital compression testing machine at a rate of 1.0 kN/s until failure. Water absorption was also determined at 28 days of age according to ASTM C642.[30] In addition, the drying shrinkage measurements were taken on mortar composites having a size of 40 mm × 40 mm × 160 mm using PMF series mold strain gauges and a data logger from Tokyo Measuring Instruments Laboratory Co., Ltd.

Atomistic Modeling. The molecular dynamics models' construction and parameters were as follows. The main hydration product of OPC, calcium silicate hydrate (CSH), was simulated using the 11 Å tobermorite crystal proposed by Hamid.[31] This structure has lattice parameters of a = 6.732 Å, b = 7.369 Å, c = 22.680 Å, $\alpha = \beta = 90°$, and

https://doi.org/10.1021/acsanm.4c05322
ACS Appl. Nano Mater. XXXX, XXX, XXX−XXX

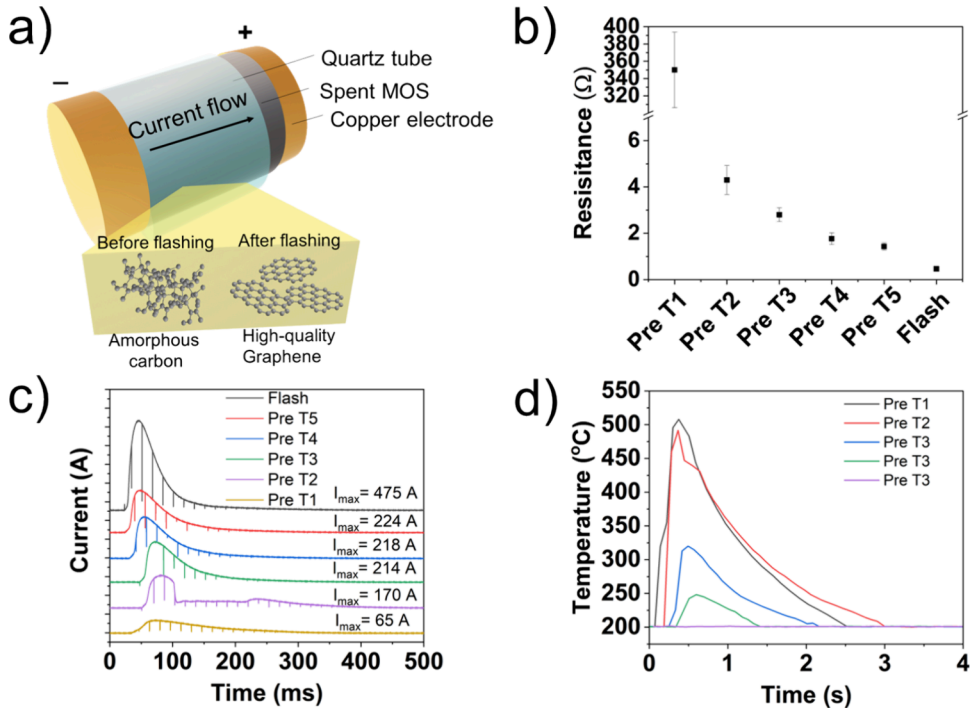

Figure 1. Synthesis of MOS-FG: (a) Schematic of the FJH process for the graphitization of MOS. (b) Resistivity values of the MOS sample during the FJH process. Error bars represent the standard deviation of 3 samples. (c) Current through the carbon source during FJH is complete in the millisecond time scale. The flash rate can be tuned by controlling the sample compression between the electrodes, which changes the sample conductivity and reaction time. (d) Time−temperature graph of FG reacted with different pretreatments. Pre = pretreatment voltage pulse.

γ = 123.180°. The built CSH was cleaved along the [001] direction[32] and then periodically replicated along the x and y directions. The sand material was simulated by using the SiO_2 crystal structure. Since the characterization findings of MOS-FG, including the Raman spectra and XRD results, indicated that the FG is turbostratic and can easily exfoliate upon sonication, FG was modeled as a monolayer.[33] Two models were constructed: first, the cement mortar, without FG, which was composed of CSH gel and SiO_2 (denoted as CSH-Si); and second, the graphene−cement mortar, where a graphene layer was added to the model (denoted as CSH-FG-Si). These two models simulated the mortar mixtures without and with FG (M1-ref and M2-FG), respectively, which were experimentally investigated. The cell size of the CSH-Si was 20.196 × 20.196 × 40.239 Å^3, while that of the CSH-FG-Si had a cell size of 20.196 × 20.196 × 43.639 Å^3. The individual components and their associated built models were first optimized using the smart algorithm. Then, the models were equilibrated under the NPT ensemble at a temperature and pressure of 298.00 K and 0.0001 GPa, respectively, using the Andersen and Berendsen controlling methods. A production run using the NVT ensemble was then performed on the models for a time of 300 ps with a time step of 1.0 fs. The COMPASS force field was used in all the simulation processes.[34] The electrostatic and van der Waals interactions were calculated by using the Ewald and atom-based summation methods, respectively. The Ewald accuracy and cutoff distance were set at 1 × 10^{-5} kcal mol^{-1} and 12.5 Å, respectively. The Materials Studio software was used in all of the simulations, and the runs were performed using the high-performance computer at ICTC-KFUPM.

RESULTS AND DISCUSSION

Flash Graphene Synthesis and Characterization. Graphene was synthesized via the FJH method. The MOS was compressed between two copper electrodes (Figure 1a) in a quartz tubes. The samples were compressed to obtain a resistivity of ≤ 500 Ω for ∼0.25 g of MOS. Given the high initial resistivity of the carbon source, five pretreatment flashes (500 ms each) at relatively low voltage (100 V) were required to carbonize the soot and increase the conductivity of the carbon precursor prior to the conversion to graphene (Figure 1b). Alternatively, small amounts of carbon black (CB, 5−10 wt %) can be mixed with the soot prior to the pretreatment to lower the initial resistivity of the starting materials. After pretreatment, the sample was flashed at 160 V to graphitize the carbon and form FG. The current through the sample was measured for each discharge (Figure 1c), which showed that the flashing process occurred in milliseconds to produce turbostratic graphene. While current measured in pretreatments does not exceed 200 A, the measured current during flashing was found to reach up to 500 A. Due to the high current discharge during flashing, it is known that the temperature of the reaction reaches up to 3000 K,[21] while the pretreatment temperature at the different pretreatment flashes was found not to exceed 550 °C (Figure 1d). The first treatment resulted in the highest spike in temperature due to the high resistive heating. However, as the carbon resistivity decreases with pretreatments, the temperature increase is less pronounced.

Like MOS, DP collected from diesel particle filters was flashed using the FJH technique to obtain high-quality graphene. The Raman spectrum of FG derived from MOS and DP (Figure 2a) shows a sharp 2D peak occurring at ∼2700 cm^{-1}, a G band occurring at ∼1580 cm^{-1}, and a small 2D band at 1350 cm^{-1}. A large I_{2D}/I_G peak ratio of 8−10 was observed for the formed FG, which indicates high crystallinity and a small degree of defect of the FG sheets (Figure 2a).[35,36] These characteristic Raman spectrum FG peaks were not present in the MOS and DP Raman spectra prior to flashing, indicating the successful conversion of amorphous carbon to graphene. This demonstrates the usefulness of the FJH process in

https://doi.org/10.1021/acsanm.4c05322
ACS Appl. Nano Mater. XXXX, XXX, XXX−XXX

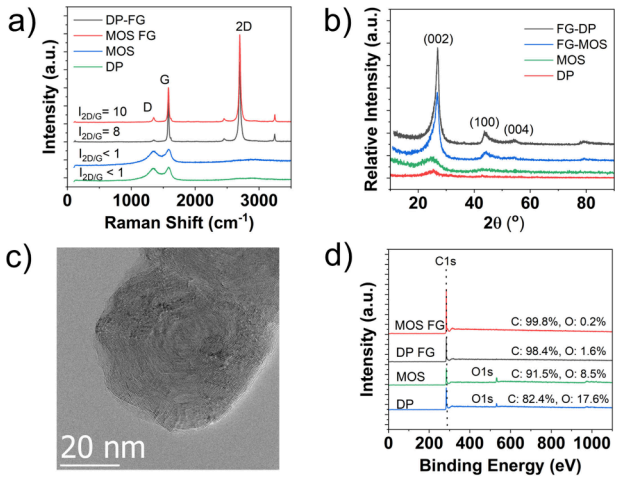

Figure 2. Characterization of MOS-FG: (a) Raman spectra of MOS and DP before and after flashing; (b) XRD profile of DP before and after flashing; (c) HR-TEM image of MOS-FG showing the layer structure of FG; (d) XPS spectra of MOS-G, DP-FG, MOS, and DP.

upgrading low-value soot from potentially any combustion process to FG.

XRD analysis of the produced FG confirmed the formation of turbostratic FG, evident by the large full width at half-maximum (fwhm) of the (200) peak at ~27° when compared to graphite nanoplatelets, which typically have a sharper (200) peak at ~26°.[23] In addition, the interlayer peaks, (101) and (102), were low in intensity due to decoupling in the graphene sheets originating from layer rotation.[37] The graphene XRD signal peaks are missing for the initial feedstock prior to flashing due to the amorphous nature of the MOS and DP. A transmission electron microscope image of the MOS-FG shows highly graphitized particles with clear graphitic layers and an interlayer spacing of 4.5 Å (Figure S1). X-ray photoelectron microscopy (XPS) analysis of the carbon feedstocks prior to flashing showed a high oxygen content. The oxygen content decreased upon flashing due to the high flashing temperature of ~3000 K,[21] resulting in full carbonization of the samples and sublimation of non-carbon elements, which was observed as outgassing.[23]

Preparation and Properties of FG-Reinforced Cement Mortar. The FG resulting from the MOS was used as an additive in cement composite mixtures. The diesel particulates were collected from a truck yard, and low quantities were obtained, which were not sufficient to make the cement composite. Before being incorporated into a composite mortar, the MOS-FG underwent bath sonication in water to ensure a uniform and homogeneous blend. The preparation of the composite is discussed in the Experimental Methods section. The mixture proportions of the mortars are tabulated in Table 2. The flow of mortars with and without the inclusion of FG was measured by using a flow table test. The flow values of the control mixture and the FG-reinforced mixture were found to be 56.9 ± 1.3% and 49.6 ± 0.8%, respectively. This indicates that the mortar admixed with FG was 13% more viscous than the control mixture (Table 2). This increase in viscosity can be attributed to the higher specific surface area of graphene materials.[11] The nanomaterials are characterized by having a large surface area, requiring a higher water content for wetting. In addition, the possibility of the presence of nanomaterial agglomerates on a large scale may lead to higher viscosity of the cement matrix.[38] Similar behavior has been reported in the literature, where decreasing fluidity increases the viscosity of a mixture, reducing its rheological properties.[4,8]

The mechanical properties of the control and FG-reinforced mortar mixtures, including the compressive, flexural, and tensile strengths, and the modulus of elasticity were studied. Figure 3a shows the compressive strength of the mixtures with

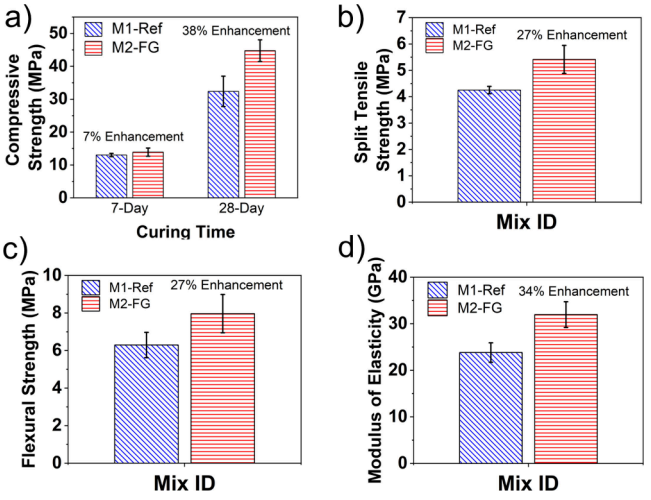

Figure 3. Mechanical properties of mixtures: (a) compressive strengths at 7 and 28 days; (b) split tensile strength at 28 days; (c) flexural strength at 28 days; and (d) modulus of elasticity at 28 days; error bars represent the standard deviation of 3 samples.

and without graphene at 7 and 28 days. As expected, the compressive strength increased with the curing time. The compressive strengths of FG-reinforced mortar (M2-FG mixture) at 7 and 28 days were higher by 6.6% and 38%, respectively, than the control mortar mixture (M1-ref mixture). In a similar trend, the M2-FG mortar showed an increase in the 28-day tensile and flexural strength by 27% and 27%, respectively, with respect to the mortar without FG (Figures 3b and 3c). Furthermore, the 28-day modulus of elasticity of FG-reinforced mortar increased by 34% compared with the control mortar mixture. The enhanced mechanical performance of cement composites reinforced with FG can be attributed to various factors. These include the nanofiller effect, which subdivides and fills coarse pores, transforming them into fine pores; the nucleation effect, which mitigates the large specific surface area of graphene by clustering particles; the acceleration of the cement hydration reaction, facilitating faster curing; and the bridging effect of graphene, impeding the formation and spread of microcracks.[4,39]

The improved mechanical strength of FG-reinforced cement composites can lead to economic and environmental advantages due to the reduction of cement consumption. When the strength of a material is improved, the required section area of a structural member can be reduced, inferring a saving of cementitious material. Based on the enhancement in the mechanical properties of the FG−cement composite, 0.1 wt % FG addition to the cementitious composite could result in a 19% reduction in the consumption of cement, which would lower both the cement's carbon footprint and the cost of building materials.

The durability characteristics of the mortars were evaluated in terms of water absorption as an intrinsic property and drying shrinkage as a dimensional stability property. Figure 4a depicts

https://doi.org/10.1021/acsanm.4c05322
ACS Appl. Nano Mater. XXXX, XXX, XXX−XXX

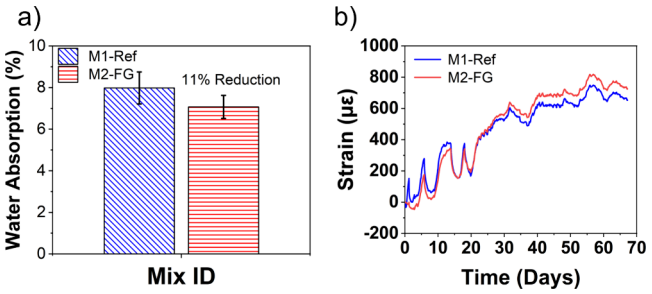

Figure 4. Durability characteristics and shrinkage of mortar mixtures: (a) water absorption; error bars represent the standard deviation of 3 samples; and (b) shrinkage measurements over time.

the 28-day water absorption of mixtures. The water absorption values of the mortar mixtures with and without FG were found to be 8% and 7.1%, respectively. Thus, the FG-reinforced mortar showed a slightly lower surface absorption relative to the control mortar mixture, presumably due to the hydrophobicity of FG. Previous studies have reported that the carbon nanosheets act as a protective coat, which enhances the resistance to water ingression.[40] In addition, the FG acts as a filler material, filling the voids at a nanolevel and avoiding further absorption of water molecules. The addition of FG influences the transport properties in the cement matrix, which improves the gel pores and strengthens the microstructure of the matrix,[10] as will be discussed in the next section.

The drying shrinkage vs time plots of mortars with and without FG are shown in Figure 4b. Both mixtures exhibited similar behavior; the mortar reinforced with FG exhibited a slight decrease in shrinkage during the early-stage monitoring period. The drying shrinkage is intricately linked to the internal pore structure and capillary channels of the matrix. By reducing porosity during the drying and water loss process, the drying shrinkage can be mitigated.[41] Therefore, the bridging effect of graphene sheets over nano- and micropores in the matrix plays a crucial role in controlling drying shrinkage.[11] At the later stages, beyond 30 days, M2-FG reversed its behavior and showed a slightly higher shrinkage. The shrinkage strains of M1-ref and M2-FG at 28 days were 523 and 547 $\mu\varepsilon$, respectively, which is slightly higher than the limit of 500 $\mu\varepsilon$ at 28 days of curing, as specified by ASTM C157.[42] In addition, the long-term shrinkage measurements of mixtures were much lower than the limit of 1000 $\mu\varepsilon$ at 56 days, as stipulated by the Australian Standard-1379.[43]

Molecular Dynamic Simulation. The atomistic modeling using molecular dynamics simulation was carried out to investigate the graphene−cement composites and their enhancement mechanisms.[44,45] Initially, the stability of the models was examined by the fluctuations of temperature and energy over the simulation time, as depicted in Figure S2. The constructed configuration models of mortar (without FG) and FG-reinforced mortar (Figure 5a,b) show the interactions between the CSH, from the Portland cement, silica (SiO_2) from the sand, and flash graphene from MOS. The horizontal concentration profiles of the different layers in the mortar model were found to be in the range of 0 to 26 Å and 25 to 42 Å, for CSH and SiO_2, respectively (Figure 5c). These concentrations are close to those in the FG-reinforced matrix model, with a relatively large concentration of the FG layer at 31.3 Å, observed as a sharp peak of the FG concentration (Figures 5b and 5d). The intensity profile of atoms along the *z*-direction after simulation is shown in Figures 5e and f. The C

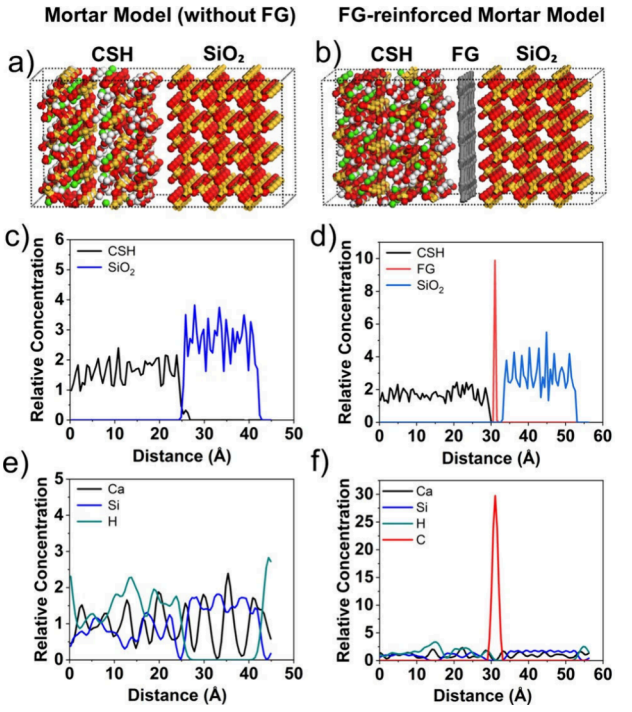

Figure 5. Initial configuration of models: (a) mortar model (CSH-SiO_2) and (b) FG-reinforced model (CSH-FG-SiO_2) and their corresponding concentration profiles (c and d). Intensity profile of atoms in the (e) mortar model (CSH-SiO_2) and (f) FG-reinforced model (CSH-FG-SiO_2) CSH-Si and (b) CSH-FG-Si.

atoms of FG are concentrated in the interfacial region with a few Ca and H atoms, which appear to be overlapping in this zone, indicating that graphene sheets reside in the interlayer region between the CSH and SiO_2.[46,47]

The local structure of the investigated models was further studied by the radial distribution function (RDF) method to reveal the nature of the interactions between cement mortar and graphene-based materials.[48] The RDF formula suggested by Hansen and McDonald[49] was used in this study, as expressed in eq 1:

$$g_{AB}(r) = \frac{1}{\langle \rho_B \rangle_{local}} \frac{1}{N_A} \sum_{i \in A}^{N_A} \sum_{i \in B}^{N_B} \frac{\delta(r_{ij} - r)}{4\pi r^2} \quad (1)$$

where $g_{AB}(r)$ is the probability of finding particle *B* within the range around particle *A*; *r* and *N* are the distance between each atom pair and the number of atoms, respectively, and $\langle \rho_B \rangle_{local}$ represents the density of *B* particles averaged over all shells around particle *A*.

Figures 6a,b show the local structure of the models, where the atoms of CSH, SiO_2, and FG interact, while Figures 6c and 6d indicate the nature of these interactions using the RDF analysis. The RDF of Ca_{CSH} and Si_{SiO_2} interaction lengths of the control mortar (M1-ref) and M2-FG model was found to be 3.0 and 2.75 Å, respectively (Figure 6c). This suggested that the presence of FG boosted the Ca−Si interactions, which resulted in a shorter interaction distance. In addition, the registered atomic bond lengths fall in the chemisorption range of 1 to 3.5 Å.[50] The interactions between the carbon of FG and Ca and O atoms of CSH (Figure 6d) showed that the Ca atoms tend to form strong interactions with FG as characterized by a horizontal ordinate and intensity of the

https://doi.org/10.1021/acsanm.4c05322
ACS Appl. Nano Mater. XXXX, XXX, XXX−XXX

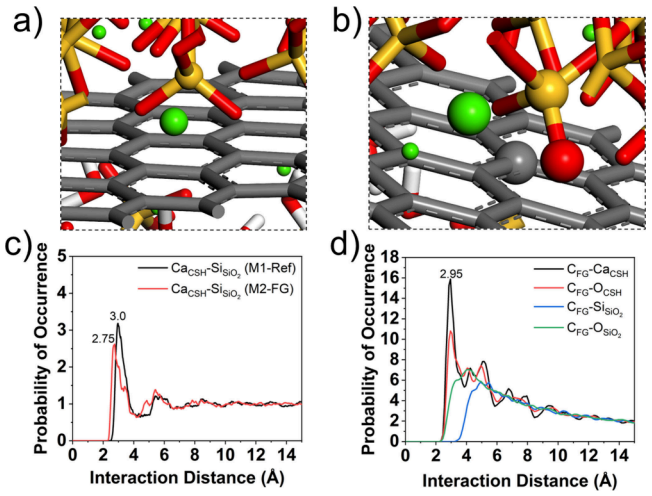

Figure 6. (a, b) Local structure snapshots showing the interaction between different atoms with FG; (c) RDF between Ca_{CSH} and Si_{SiO_2} for both models; and (d) RDF between C_{FG} and different atoms of the cement mortar system.

first prominent peak. This could be due to the formation of charge attraction between the calcium atoms, which are electron deficient, and the graphene sheets, which are electron rich. The O atoms of CSH behaved similarly but with a lower occurrence intensity. Conversely, the RDF curves of C_{FG} and Si and O atoms of SiO_2 had larger interaction distances with lower probability of occurrence compared to the Ca atoms of CSH, indicating that the Ca atoms play an important role in the reinforcement mechanism of FG in the cement mortar system.

The equilibrated models were then used to predict the mechanical properties of the composites. These included bulk modulus (K), shear modulus (G), Young's modulus (E), and Poisson's ratio (ν). Determination of such properties, especially K and G, through experimental methods can be difficult and/or complicated. The constant-strain method and the Voigt−Reuss−Hill rule were used to calculate the elastic moduli.[51] Table 3 lists the values of the mechanical properties

Table 3. Calculated Density and Mechanical Properties of the Models Obtained from the MD Simulation

Model	Density ρ (g/cm^3)	Bulk modulus K (GPa)	Shear modulus G (GPa)	Young's modulus E (GPa)	Poisson's ratio ν
M1-ref	2.83	41.86	18.80	49.07	0.30
M2-FG	3.28	78.94	27.14	73.05	0.35

as well as the densities of both models. The densities (ρ) of M1-ref and M2-FG were 2.83 and 3.28 g/cm^3, respectively, indicating that the mortar reinforced with FG had a higher density. In addition, the elastic moduli of M2-FG were also higher than those of M1-ref. For example, the obtained E values of M1-ref and M2-FG were found to be 49.1 and 73.1 GPa, respectively. Thus, an increase of 49% was achieved upon incorporation of FG into the mortar. The improved mechanical response of the FG-reinforced cement composite agreed well with the experimental findings. In comparison to the mechanical properties of CSH reported in the literature[52−54] the properties of M2-FG were found to be on the higher side of the reported range: K = 54.2 to 77.8 GPa, G = 29.0 to 42.4 GPa, E = 77.0 to 129.7 GPa, and ν = 0.28 to 0.32. Therefore, the molecular dynamics results provided a good estimate of the mechanical properties and supported the finding that FG enhanced the mechanical performance of the cement composite.

CONCLUSIONS

The present work explored the feasibility of upcycling waste materials, including motor oil soot and diesel particulate, to produce high-quality flash graphene. The obtained FG was used to reinforce cement mortar, where incorporating 0.1 wt % FG resulted in an enhancement in the 28-day compressive, tensile, and flexural strengths and modulus of elasticity by 38%, 27%, 27%, and 34%, respectively, compared to the cement composite without FG. The structure, dynamics, and enhancement mechanisms of FG in cement were studied using molecular dynamics simulations. The molecular dynamics results indicated that the elastic moduli of the FG-reinforced cement system were improved, with the Young's modulus increasing by ∼49%. The RDF analysis showed that Ca−Si interactions in the CSH were enhanced by the presence of FG and that chemical interactions are most likely to take place between Ca atoms of the CSH and C atoms of the FG. Overall, using FG derived from MOS in construction and building materials could conserve environmental resources, reducing cement usage.

ASSOCIATED CONTENT

Supporting Information

The Supporting Information is available free of charge at https://pubs.acs.org/doi/10.1021/acsanm.4c05322.

TEM interlayer spacing, model stability, and FJH safety guidelines (PDF)

AUTHOR INFORMATION

Corresponding Authors

Shamsad Ahmad − *Civil Engineering Department, King Fahd University of Petroleum & Minerals, Dhahran 31261, Saudi Arabia; Interdisciplinary Research Center for Construction and Building Materials, King Fahd University of Petroleum & Minerals, Dhahran 31261, Saudi Arabia;* Email: shamsad@kfupm.edu.sa

James M. Tour − *Department of Chemistry, Department of Materials Science and Nano-Engineering, and Smalley-Curl Institute, The NanoCarbon Center and the Rice Advanced Materials Institute, Rice University, Houston, Texas 77005, United States;* orcid.org/0000-0002-8479-9328; Email: tour@rice.edu

Authors

Wala A. Algozeeb − *Department of Chemistry, Rice University, Houston, Texas 77005, United States;* orcid.org/0000-0002-6394-7483

Ali Algadhib − *Civil Engineering Department, King Fahd University of Petroleum & Minerals, Dhahran 31261, Saudi Arabia; Interdisciplinary Research Center for Construction and Building Materials, King Fahd University of Petroleum & Minerals, Dhahran 31261, Saudi Arabia*

Mohammed A. Al-Osta − *Civil Engineering Department, King Fahd University of Petroleum & Minerals, Dhahran 31261, Saudi Arabia; Interdisciplinary Research Center for*

https://doi.org/10.1021/acsanm.4c05322
ACS Appl. Nano Mater. XXXX, XXX, XXX−XXX

Construction and Building Materials, King Fahd University of Petroleum & Minerals, Dhahran 31261, Saudi Arabia; orcid.org/0000-0002-3678-2695

Ashraf A. Bahraq − *Civil Engineering Department, King Fahd University of Petroleum & Minerals, Dhahran 31261, Saudi Arabia; Interdisciplinary Research Center for Construction and Building Materials, King Fahd University of Petroleum & Minerals, Dhahran 31261, Saudi Arabia*

Weiyin Chen − *Department of Chemistry, Rice University, Houston, Texas 77005, United States;* orcid.org/0000-0002-6427-4129

Syed Khaja Najamuddin − *Civil Engineering Department, King Fahd University of Petroleum & Minerals, Dhahran 31261, Saudi Arabia;* orcid.org/0000-0003-3183-7770

Syed Imran Ali − *Civil Engineering Department, King Fahd University of Petroleum & Minerals, Dhahran 31261, Saudi Arabia;* orcid.org/0000-0003-3763-099X

Complete contact information is available at: https://pubs.acs.org/10.1021/acsanm.4c05322

Author Contributions

The manuscript was written through contributions of all authors. All authors have given approval to the final version of the manuscript.

Notes

The authors declare the following competing financial interest(s): Rice University owns intellectual property, being licensed to a company in which J.M.T. is a shareholder, although he is not an officer or a director in the company. Conflicts of interest are regularly managed through disclosures to the Rice University Office of Sponsored Programs and Research Compliance. The authors declare no other potential conflicts.

■ ACKNOWLEDGMENTS

Support at Rice University includes the Air Force Office of Scientific Research (FA9550-22-1-0526) and the U.S. Army Corp of Engineers, ERDC (W912HZ-21-2-0050). W.A.A. thanks Saudi Aramco for a fellowship. We thank John Li for his help in producing the MOS. We thank Dr. Bo Chen for his help with XPS. The authors acknowledge the support received from King Fahd University of Petroleum & Minerals, Dhahran, Saudi Arabia, and Rice University, Houston, TX, USA. We also thank Waste Management, Inc., for providing us with DP samples.

■ REFERENCES

(1) Dalal, S. P.; Dalal, P. Experimental Investigation on Strength and Durability of Graphene Nanoengineered Concrete. *Constr. Build. Mater.* **2021**, *276*, No. 122236.

(2) Brodie, B. C. Xiii. On the Atomic Weight of Graphite. *Philos. Trans. R. Soc. London* **1859**, *149*, 249−259.

(3) Lee, C.; Wei, X.; Kysar, J. W.; Hone, J. Measurement of the Elastic Properties and Intrinsic Strength of Monolayer Graphene. *Science* **2008**, *321*, 385−8.

(4) Lin, Y.; Du, H. Graphene Reinforced Cement Composites: A Review. *Constr. Build. Mater.* **2020**, *265*, No. 120312.

(5) Hernández Rosas, J. J.; Ramírez Gutiérrez, R. E.; Escobedo-Morales, A.; Chigo Anota, E. First Principles Calculations of the Electronic and Chemical Properties of Graphene, Graphane, and Graphene Oxide. *J. Mol. Model.* **2011**, *17*, 1133−1139.

(6) Yang, H.; Cui, H.; Tang, W.; Li, Z.; Han, N.; Xing, F. A Critical Review on Research Progress of Graphene/Cement Based Composites. *Composites, Part A* **2017**, *102*, 273−296.

(7) Shamsaei, E.; de Souza, F. B.; Yao, X.; Benhelal, E.; Akbari, A.; Duan, W. Graphene-Based Nanosheets for Stronger and More Durable Concrete: A Review. *Constr. Build. Mater.* **2018**, *183*, 642−660.

(8) Devi, S. C.; Khan, R. A. Effect of Graphene Oxide on Mechanical and Durability Performance of Concrete. *J. Build. Eng.* **2020**, *27*, No. 101007.

(9) Suo, Y.; Guo, R.; Xia, H.; Yang, Y.; Zhou, B.; Zhao, Z. A Review of Graphene Oxide/Cement Composites: Performance, Functionality, Mechanisms, and Prospects. *J. Build. Eng.* **2022**, *53*, No. 104502.

(10) Mohammed, A.; Sanjayan, J. G.; Duan, W. H.; Nazari, A. Incorporating Graphene Oxide in Cement Composites: A study of Transport Properties. *Constr. Build. Mater.* **2015**, *84*, 341−347.

(11) Ho, V. D.; Gholampour, A.; Losic, D.; Ozbakkaloglu, T. Enhancing the Performance and Environmental Impact of Alkali-Activated Binder-Based Composites Containing Graphene Oxide and Industrial by-Products. *Constr. Build. Mater.* **2021**, *284*, No. 122811.

(12) Bellum, R. R.; Muniraj, K.; Indukuri, C. S.; Madduru, S. R. Investigation on Performance Enhancement of Fly Ash-GGBFS Based Graphene Geopolymer Concrete. *J. Build. Eng.* **2020**, *32*, No. 101659.

(13) Pan, Z.; He, L; Qiu, L.; Korayem, A. S.; Li, G.; Zhu, J. W.; Collins, F.; Li, D.; Duan, W. H.; Wang, M. C. Mechanical Properties and Microstructure of a Graphene Oxide-Cement Composite. *Cem. Concr. Compos.* **2015**, *58*, 140−147.

(14) Lv, S.; Ting, S.; Liu, J.; Zhou, Q. Use of Graphene Oxide Nanosheets to Regulate the Microstructure of Hardened Cement Paste to Increase its Strength and Toughness. *Cryst. Eng. Comm.* **2014**, *16*, 8508−8516.

(15) Birenboim, M.; Nadiv, R.; Alatawna, A.; Buzaglo, M.; Schahar, G.; Lee, J.; Kim, G.; Peled, A.; Regev, O. Reinforcement and Workability Aspects of Graphene-Oxide-Reinforced Cement Nanocomposites. *Compos. B Eng.* **2019**, *161*, 68−76.

(16) Qureshi, T. S.; Panesar, D. K.; Sidhureddy, B.; Chen, A; Wood, P. C. Nano-Cement Composite with Graphene Oxide Produced from Epigenetic Graphite Deposit. *Compos. B Eng.* **2019**, *159*, 248−258.

(17) Yin, B.; Wu, C.; Hou, D.; Li, S.; Jin, Z.; Wang, M.; Wang, X. Research and Application Progress of Nano-Modified Coating in Improving the Durability of Cement-based Materials. *Prog. Org. Coatings.* **2021**, *161*, No. 106529.

(18) Wu, Y. H.; Yu, T.; Shen, Z. X. Two-Dimensional Carbon Nanostructures: Fundamental Properties, Synthesis, Characterization, and Potential Applications. *J. Appl. Phys.* **2010**, *108*, No. 071301.

(19) Yi, M.; Shen, Z. A Review on Mechanical Exfoliation for the Scalable Production of Graphene. *J. Mater. Chem. A* **2015**, *3*, 11700−11715.

(20) Hernandez, Y.; Nicolosi, V.; Lotya, M.; Blighe, F. M.; Sun, Z.; De, S.; McGovern, I. T.; Holland, B.; Byrne, M.; Gun'Ko, Y. K.; Boland, J. J.; Niraj, P.; Duesberg, G.; Krishnamurthy, S.; Goodhue, R.; Hutchison, J.; Scardaci, V.; Ferrari, A. C.; Coleman, J. N. High-Yield Production of Graphene by Liquid-Phase Exfoliation of Graphite. *Nat. Nanotechnol.* **2008**, *3*, 563−568.

(21) Luong, D. X.; Bets, K. V.; Algozeeb, W. A.; Stanford, M. G.; Kittrell, C.; Chen, W.; Salvatierra, R. V.; Ren, M.; McHugh, E. A.; Advincula, P. A.; Wang, Z.; Bhatt, M.; Guo, H.; Mancevski, V.; Shahsavari, R.; Yakobson, B. I.; Tour, J. M. Gram-Scale Bottom-up Flash Graphene Synthesis. *Nature* **2020**, *577*, 647−651.

(22) Advincula, P. A.; Granja, V.; Wyss, K. M.; Algozeeb, W. A.; Chen, W.; Beckham, J. L.; Luong, D. X.; Higgs, C. F.; Tour, J. M. Waste Plastic- and Coke-Derived Flash Graphene as Lubricant Additives. *Carbon* **2023**, *203*, 876−885.

(23) Algozeeb, W. A.; Savas, P. E.; Luong, D. X.; Chen, W.; Kittrell, C.; Bhat, M.; Shahsavari, R.; Tour, J. M. Flash Graphene from Plastic Waste. *ACS Nano* **2020**, *14*, 15595−15604.

(24) Advincula, P.; Luong, D.; Chen, W.; Raghuraman, S.; Shahsavari, R.; Tour, J. M. Flash Graphene from Rubber Waste. *Carbon* **2021**, *178*, 649−656.

(25) ASTM International, *ASTM C150/C150m-18: Standard Specification for Portland Cement*, 2019.

(26) ASTM International, *ASTM C1437-15: Standard Test Method for Flow of Hydraulic Cement Mortar*, West Conshohocken, PA, 2015.
(27) ASTM International, *ASTM C109/C109m-16a: Standard Test Method for Compressive Strength of Hydraulic Cement Mortars*, 2016, pp 1−10.
(28) ASTM International, *ASTM C78/C78M: Standard Test Method for Flexural Strength of Concrete (Using Simple Beam with Third-Point Loading)*, West Conshohocken, 2018.
(29) ASTM International, *ASTM C496: Standard Test Method for Splitting Tensile Strength of Cylindrical Concrete Specimens*, 2017.
(30) ASTM International, *ASTM C642: Standard Test Method for Density, Absorption, and Voids in Hardened Concrete*, West Conshohocken, PA, 2013.
(31) Hamid, S. A. The Crystal Structure of the 11 Å Natural Tobermorite Ca_2. 25 $[Si_3O_7$. 5 $(OH)_{1.5}]\cdot 1H_2O$. *Z. fur Krist. Cryst. Mater.*. **1981**, *154*, 189−198.
(32) Hou, D.; Yu, J.; Liu, Q.-f.; Dong, B.; Wang, X.; Wang, P.; Wang, M. Nanoscale Insight on the Epoxy-Cement Interface in Salt Solution: A Molecular Dynamics Study. *Appl. Surf. Sci.* **2020**, *509*, No. 145322.
(33) Bahraq, A. A.; Al-Osta, M. A.; Obot, I. B.; Baghabra Al-Amoudi, O. S.; Saleh, T. A.; Maslehuddin, M. Improving the Adhesion Properties of Cement/Epoxy Interface Using Graphene-Based Nanomaterials: Insights From Molecular Dynamics Simulation. *Cem. Concr. Compos.* **2022**, *134*, No. 104801.
(34) Sun, H. Compass: An *Ab Initio* Force-Field Optimized for Condensed-Phase Applicationsoverview with Details on Alkane and Benzene Compounds. *J. Phys. Chem. B* **1998**, *102*, 7338−7364.
(35) Cançado, L. G.; Takai, K.; Enoki, T.; Endo, M.; Kim, Y. A.; Mizusaki, H.; Jorio, A.; Coelho, L. N.; Magalhães-Paniago, R.; Pimenta, M. A. General Equation for the Determination of the Crystallite Size La of Nanographite by Raman Spectroscopy. *Appl. Phys. Lett.* **2006**, *88*, No. 163106.
(36) Schmucker, S. W.; Cress, C. D.; Culbertson, J. C.; Beeman, J. W.; Dubon, O. D.; Robinson, J. T. Raman Signature of Defected Twisted Bilayer Graphene. *Carbon* **2015**, *93*, 250−257.
(37) Li, Z. Q.; Lu, C. J.; Xia, Z. P.; Zhou, Y.; Luo, Z. X-Ray Diffraction Patterns of Graphite and Turbostratic Carbon. *Carbon* **2007**, *45*, 1686−1695.
(38) Shang, Y.; Zhang, D.; Yang, C.; Liu, Y.; Liu, Y. Effect of Graphene Oxide on the Rheological Properties of Cement Pastes. *Constr. Build. Mater.* **2015**, *96*, 20−28.
(39) Zhang, P.; Wang, M.; Han, X.; Zheng, Y. A Review on Properties of Cement-Based Composites Doped with Graphene. *J. Build. Eng.* **2023**, *70*, No. 106367.
(40) Safarkhani, M.; Naderi, M. Enhanced Impermeability of Cementitious Composite by Different Content of Graphene Oxide Nanoparticles. *J. Build. Eng.* **2023**, *72*, No. 106675.
(41) Gao, Y.; Luo, J.; Yuan, S.; Zhang, J.; Gao, S.; Zhu, M.; Li, Z.; Zhou, X. Fabrication of Graphene Oxide/Fiber Reinforced Polymer Cement Mortar with Remarkable Repair and Bonding Properties. *J. Mater. Res/ Technol.* **2023**, *24*, 9413−9433.
(42) ASTM International, *ASTM C157: Standard Test Method for Length Change of Hardened Hydraulic-Cement Mortar and Concrete*, West Conshohocken, PA, 2008.
(43) Australian Standard, *AS 1379-2007: Specification and Supply of Concrete*; Standards Australia: Australia, 2017.
(44) Bahraq, A. A.; Al-Osta, M. A.; Al-Amoudi, O. S. B.; Saleh, T. A.; Obot, I. B. Atomistic Simulation of Polymer-Cement Interactions: Progress and Research Challenges. *Constr. Build. Mater.* **2022**, *327*, No. 126881.
(45) Bahraq, A. A.; Al-Osta, M. A.; Baghabra Al-Amoudi, O. S.; Obot, I. B.; Maslehuddin, M.; Ahmed, H.-R.; Saleh, T. A. Molecular Simulation of Cement-Based Materials and Their Properties. *Eng. J.* **2022**, *15*, 165−178.
(46) Hou, D.; Lu, Z.; Li, X.; Ma, H.; Li, Z. Reactive Molecular Dynamics and Experimental Study of Graphene-Cement Composites: Structure, Dynamics and Reinforcement Mechanisms. *Carbon* **2017**, *115*, 188−208.
(47) Zhang, Y.; Yang, T.; Jia, Y.; Hou, D.; Li, H.; Jiang, J.; Zhang, J. Molecular Dynamics Study on the Weakening Effect of Moisture Content on Graphene Oxide Reinforced Cement Composite. *Chem. Phys. Lett.* **2018**, *708*, 177−182.
(48) Obot, I. B.; Bahraq, A. A.; Alamri, A. H. Density Functional Theory and Molecular Dynamics Simulation of the Corrosive Particle Diffusion in Pyrimidine and Its Derivatives Films. *Comput. Mater. Sci.* **2022**, *210*, No. 111428.
(49) Hansen, J. P.; McDonald, I. R. *Theory of Simple Liquids with Applications to Soft Matter*; Academic Press, 2013, eBook.
(50) El-Hajjaji, F.; Ech-chihbi, E.; Rezki, N.; Benhiba, F.; Taleb, M.; Chauhan, D. S.; Quraishi, M. A. Electrochemical and Theoretical Insights on the Adsorption and Corrosion Inhibition of Novel Pyridinium-Derived Ionic Liquids for Mild Steel in 1 M HCl. *J. Mol. Liq.* **2020**, *314*, No. 113737.
(51) Elasticity of Structures. In *Structure, Deformation, and Integrity of Materials*; Wiley, 2006; pp 307−336.
(52) Dharmawardhana, C. C.; Misra, A.; Aryal, S.; Rulis, P.; Ching, W. Y. Role of Interatomic Bonding in the Mechanical Anisotropy and Interlayer Cohesion of CSH Crystals. *Cem. Concr. Res.* **2013**, *52*, 123−130.
(53) Hajilar, S.; Shafei, B. Nano-Scale Investigation of Elastic Properties of Hydrated Cement Paste Constituents Using Molecular Dynamics Simulations. *Comput. Mater. Sci.* **2015**, *101*, 216−226.
(54) Shahsavari, R.; Buehler, M. J.; Pellenq, R. J. M.; Ulm, F.-J. First-Principles Study of Elastic Constants and Interlayer Interactions of Complex Hydrated Oxides: Case Study of Tobermorite and Jennite. *J. Am. Ceram. Soc.* **2009**, *92*, 2323−2330.

https://doi.org/10.1021/acsanm.4c05322
ACS Appl. Nano Mater. XXXX, XXX, XXX−XXX